ChemComm

Accepted Manuscript

This article can be cited before page numbers have been issued, to do this please use: X. Liu, Y. Tian, H. Cui and H. Fan, *Chem. Commun.*, 2018, DOI: 10.1039/C8CC04456B.

ROYAL SOCIETY OF CHEMISTRY

rsc.li/chemcomm

View Article Online
DOI: 10.1039/C8CC04456B

Journal Name

COMMUNICATION

Received 00th January 20xx,
Accepted 00th January 20xx

DOI: 10.1039/x0xx00000x

www.rsc.org/

The influence of NHCs on C–Si and C–C reductive elimination: A computational study of the selectivity of Ni-catalyzed C–H activation of arenes with vinylsilanes†

Xiao-Jun Liu,* Ying-Ying Tian, Hong-Qiang Cui, and Hui-Jun Fan

Density functional theory calculations were performed to investigate the mechanism and origins of NHC-controlled selectivity of Ni-catalyzed C–H activation of arenes with vinylsilanes. The key to the selectivity is the different impact of NHCs on the C–Si/C–C reductive elimination of the square-planar/T-shaped intermediate.

Silyl-substituted aromatic compounds are commonly used in synthetic chemistry, pharmaceuticals, material, and polymer science.[1] Traditionally, arylsilanes are obtained by addition of chlorosilanes to Grignard reagents,[2] while this method is limited by the functional group incompatibility. By prefunctionalization of the arene, arylsilanes can be alternatively prepared by transition-metal-catalyzed cross-coupling of aryl halides with hydrosilanes[3] or disilanes.[4] In this context, direct C–H silylation of arenes with hydro- or vinylsilane represents an efficient and waste-minimizing access to organosilanes.[5]

The past few years have witnessed the development of C–H activation and functionalization by using earth-abundant first-row transition metals such as Ni.[6] Design, optimization and fine-tuning of the ligand structure have proven to be crucial for Ni-catalyzed reactions.[7] In a recent example, Johnson reported the Ni(0)-catalyzed C–H silylation of arenes with vinylsilanes, in which the choice of *N*-heterocyclic carbene (NHC) donors plays a vital role in the selectivity of the reaction (Scheme 1).[8] The reaction of C_6F_5H and $H_2C{=}CHSiMe_3$ with nickel complex **cat1** yields the silylation product $C_6F_5SiMe_3$ (**P1**), while the catalytic complex **cat2** gives the unwanted alkene hydroarylation product **P2**. The proposed catalytic cycle for the silylation and hydroarylation is described in Scheme 2. For the reaction with **cat1**, the experimental isotope labelling studies suggest that

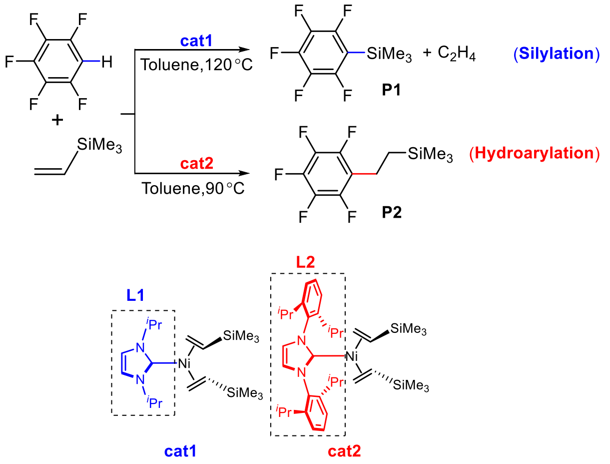

Scheme 1. Ni(0)-catalyzed C–H silylation and hydroarylation of arenes with vinylsilanes reported by Johnson.[8]

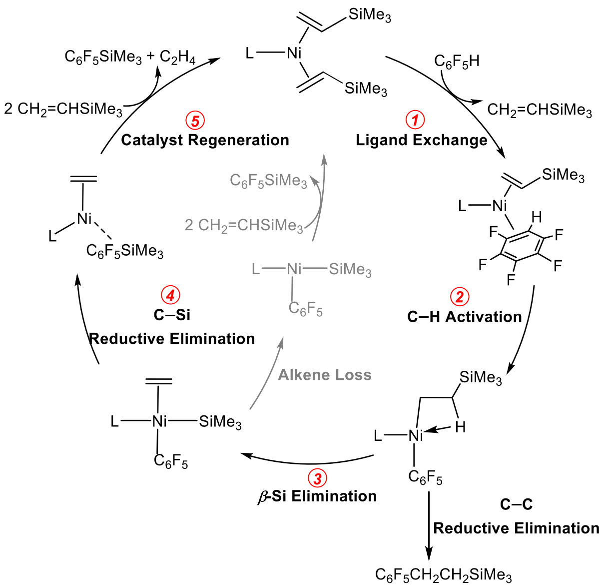

Scheme 2. Catalytic cycle for Ni-catalyzed C–H silylation and hydroarylation.

College of Chemistry, Chemical Engineering and Materials Science, Collaborative Innovation Center of Functionalized Probes for Chemical Imaging in Universities of Shandong, Key Laboratory of Molecular and Nano Probes, Ministry of Education, Institute of Molecular and Nano Science, Shandong Normal University, Jinan 250014, P. R. China. E-mail: xiaojunliu@sdnu.edu.cn.

† Electronic Supplementary Information (ESI) available: Computational details, additional results and Cartesian coordinates of all optimized structures. See DOI: 10.1039/x0xx00000x

both the C–H activation and β-Si elimination are reversible and not rate limiting. However, whether the alkene loss occurs prior to C–Si reductive elimination and the rate-determining step cannot be determined. More importantly, how the NHCs tune the competing C–Si and C–C reductive elimination remain to be explored.

The catalyst first undergoes ligand substitution for C_6F_5H, generating the substrate-coordinated complex **2**. The substitution reactions for **cat1** (**L1**) and **cat2** (**L2**) are endergonic by 7.9 and 17.9 kal/mol (Fig. 1), respectively. The subsequent C–H activation occurs via the ligand-to-ligand hydrogen transfer (LLHT)[9] transition state **TS1**, in which the oxidative addition is coupled with insertion process. The C–H activation is reversible and requires a 16.7 (20.3) kcal/mol barrier from **cat1** (**cat2**), which agrees well with experimental observation. In addition, the hydrogen transfer to 2-site of $H_2C{=}CHSiMe_3$ can also occur, but the following reductive elimination requires a much higher barrier (see ESI†).

In Pd(0) and Pt(0) complexes, the C–H activation occurs through concerted oxidative addition of the C–H bond to the metal, affording the metal hydride intermediate. However, the C–H activation in the Ni(0) analogue happens via the LLHT mechanism. The preference for LLHT in the Ni(0) complex can be attributed to the smaller atomic radius and weaker Ni(II)–H bond.[9b] Fig. 2A shows the electronic energy and natural population analysis (NPA) charges of Ni and transferring H along the intrinsic reaction coordinate of **TS1-L1**. Different from the curve of concerted metalation-deprotonation (CMD) mechanism,[10] the energy curve of the LLHT is relatively smoother. The charge of Ni gradually increases, which is consistent with that the formal oxidation state of Ni changes from 0 to +2 during the oxidative addition. It is noteworthy that the charge of H decreases nearly to zero around the transition state and then increases with further transfer. We next chose three representative points in Fig. 2A to investigate the changes of localized orbital locator (LOL)[11] to get a vivid electronic picture (Fig. 2B). At shorter C(aryl)–H distance (point X), the localization region between the two carbons of $H_2C{=}CHSiMe_3$ is featured with ($\sigma + \pi$) character, while the region becomes mainly C–C σ bond at point Z. Fig. 2B also clearly reveals the formation of the two new Ni–C bonds. In transition state **TS1-L1** (point Y), the electron is mainly localized around the transferring H instead of the middle region between Ni and H, which is in accordance with the calculated charge of H.

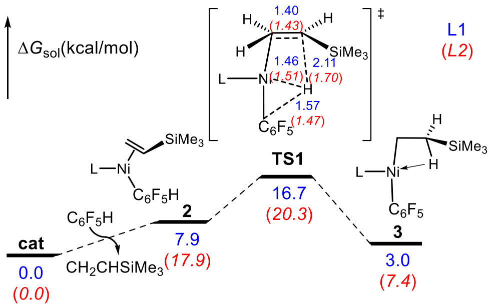

Fig. 1 Free energy profiles for the C–H activation, with bond lengths in Å.

View Article Online
DOI: 10.1039/C8CC04456B

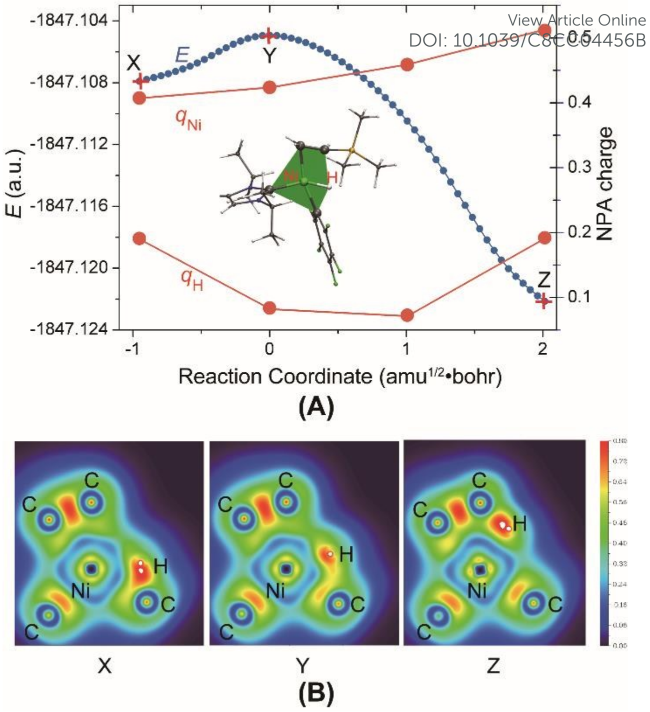

Fig. 2 (A) Electronic energies and NPA charges along the intrinsic reaction coordinate of LLHT transition state **TS1-L1**; (B) LOL function for the three selected points.

The free energy changes of the competing silylation and hydroarylation of alkylnickel aryl intermediate **3** are shown in Fig. 3. Intermediate **3** can undergo β-Si elimination via **TS2** to give the ethylene-coordinated intermediate **4**, and the subsequent C–Si reductive elimination generates the silylation product **P1**. In addition, ethylene loss may happen in **4** via **TS4** to generate **5**, and the subsequent C–Si bond formation via **TS3** yields **P1**. For **L1**, the alkene loss prior to the C–Si reductive elimination (the gray path in Fig. 3) is 2.3 kcal/mol less favorable than the direct C–Si reductive elimination (**TS4-L1** vs **TS3-L1**). Furthermore, the C–Si reductive elimination in gray path requires a much higher barrier (19.8 kcal/mol for **5-L1** to **TS5-L1**) as compared to that in the direct C–Si reductive elimination (6.8 kcal/mol for **4-L1** to **TS3-L1**). For **L2**, although the alkene loss requires similar barrier, while both **4-L2** and **TS4-L2** are higher in energies due to steric repulsions between alkene and bulky **L2**.

Alternatively, **3** can isomerize to **10**, which undergoes C–C reductive elimination to afford the hydroarylation product **P2**. In **3**, a β-C–H agostic interaction exists, and the two hydrocarbyl groups are *trans* to each other. **3** isomerizes via the Y-shaped transition state **TS6** to the T-shaped intermediate **8**, in which the Ni–C(aryl) and Ni–C(alkyl) are mutually *cis.*[12] It should be noted that **8** cannot directly undergo C(sp^2)–C(sp^3) reductive elimination to yield **11**. Instead, **8** should isomerize via **TS7** to a second β-agostic Ni intermediate **9.** For both **L1** and **L2**, the two steps of isomerization are very facile. Rotation of Ni–C(alkyl) bond in **9** results in the T-shaped intermediate **10** that is able to undergo C(sp^2)–C(sp^3) reductive elimination to yield **11**. Comparing the structures of **8** and **10**, the major difference lies

View Article Online
DOI: 10.1039/C8CC04456B

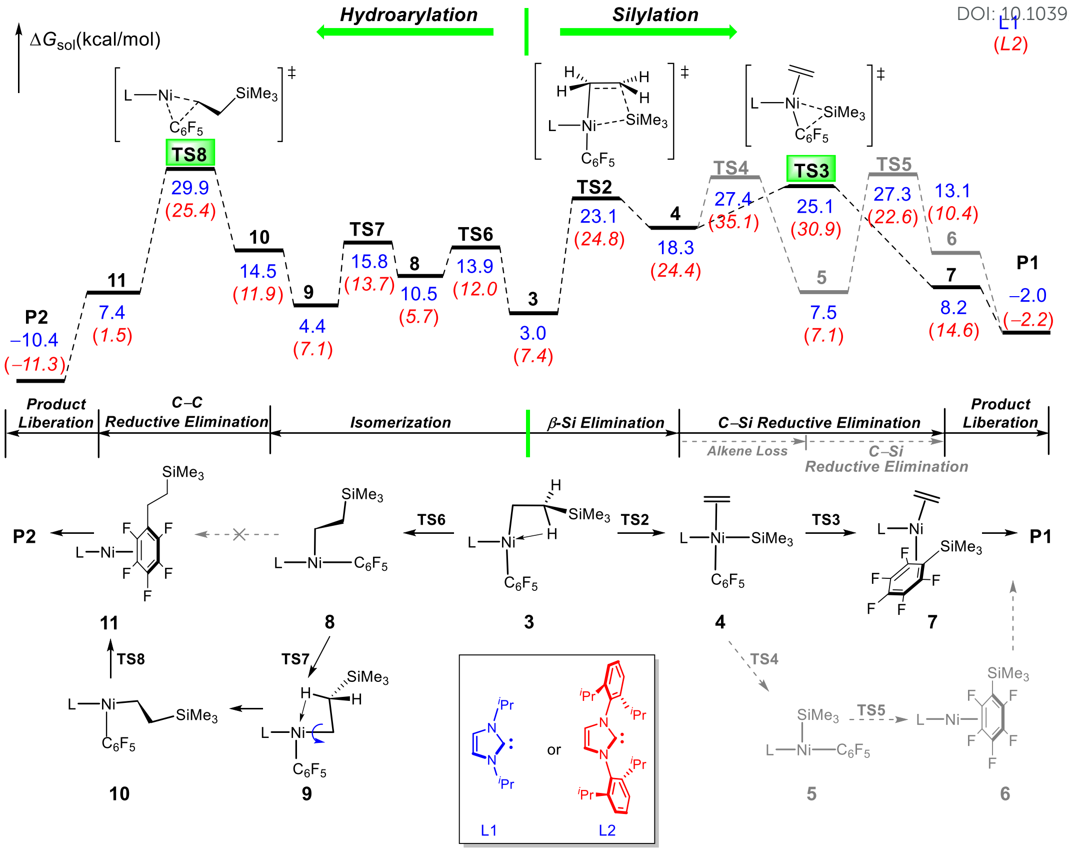

Fig. 3 Free energy profiles for the silylation and hydroarylation.

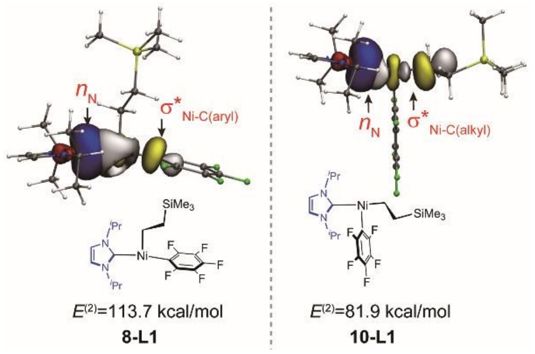

Fig. 4 Important natural bond orbital (NBO) donor-accepter interactions in **8-L1** and **10-L1** and the corresponding NBOs (isovalue = 0.05).

in the positions of alkyl and aryl relative to the NHC ligand. In **8-L1**, the C_6F_5 moiety is *trans* to **L1**, and a stronger interaction between the lone pair of carbene carbon[13] and the antibonding of Ni–C(aryl) was observed. This type of $n_C \rightarrow \sigma^*_{Ni-C(aryl)}$ delocalization ($E^{(2)}$ =113.7 kcal/mol in Fig. 4) makes C(carbene), Ni and C(aryl) nearly collinear and hinder the formation of C(sp^2)–C(sp^3) bond. However, the stabilization energy arising from the $n_C \rightarrow \sigma^*_{Ni-C(alkyl)}$ in **10-L1** is smaller (81.9 kcal/mol) due to the bigger orbital energy difference and unfavorable donor–acceptor overlap. Therefore, the C(sp^2)–C(sp^3) bond formation in **10** is more likely to happen.

Comparing the two competing pathways shown in Fig. 3, the determining transition states are the reductive elimination **TS3** and **TS8**. To further understand the origins of the ligand effects, we decrease the carbene size gradually by changing the *N*-substituents. As depicted in Fig. 5A, from **L2** to **L1′**, the energy of **TS3** decreases overall, indicating that a smaller carbene could promote the C–Si reductive elimination. The energy barrier for the C–Si bond formation mainly arises from the destabilization of the σ^- orbital shown in Fig. 5B.[14] The four-coordinate complex **4** affords the square-planar geometry, while both the $SiMe_3$ and C_6F_5 moieties deviate obviously from the ligand–Ni–ethylene plane in the succeeding **TS3**.[15] The presence of large steric repulsions between the NHC and C_6F_5 in the case of **L2** makes **TS3-L2** higher in energy, and **TS3-L1′** with the smallest ligand has the lowest energy, which is validated by the relationship between buried volumes and $\Delta G^{\neq}$(**TS3**). In the C–C reductive elimination, the intermediate **10** affords the T-shaped geometry, which is shifted towards Y-shaped geometry upon moving to **TS8**. No clear trends between the size of NHC and the energy of **TS8** can be outlined, which prompts us to consider the electronic effect of the ligands. However, the small differences within the various ligands do not provide necessary basis for further analysis. Finally, the electrostatic potential surfaces of **TS8** with **L2** and **L2′** show better electrostatic matching (Fig. 5C); that is, the more electron-deficient (blue) NCH ligands are in in close proximity to electron-rich (red) region of the C_6F_5 moiety. In

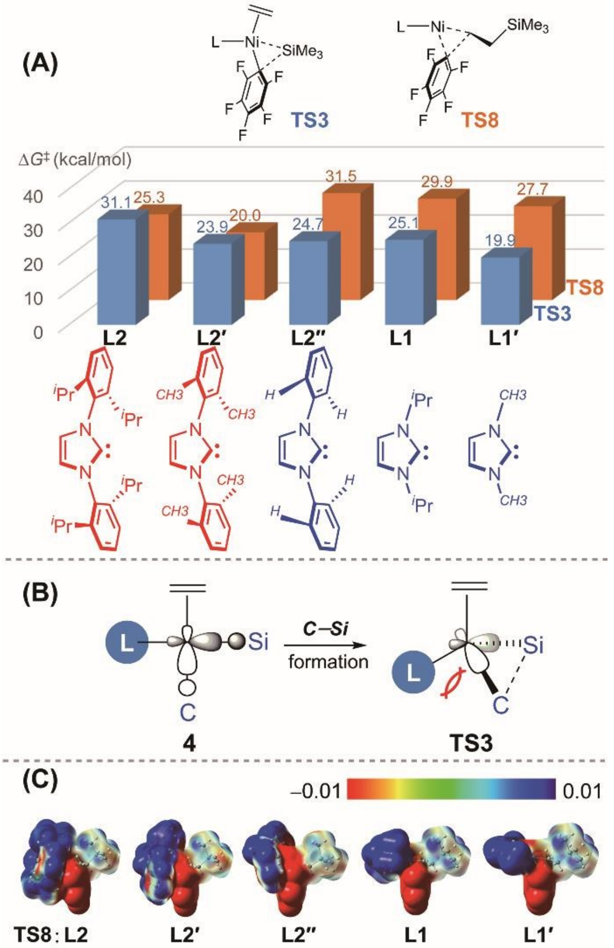

Fig. 5 (A) $\Delta G^{\ddagger}$ for **TS3** and **TS8** at 120 °C; (B) evolution of the key C–Ni–Si bonding orbital during **4**→**TS3**; (C) electrostatic potential surfaces of **TS8**.

addition, a repulsive interaction between ^{i}Pr and $SiMe_3$ is observed in **TS8-L2**, which explains its higher energy relative to **TS8-L2′**. Conversely, for **L2″**, **L1** and **L1′**, the electrostatics of the NCH and C_6F_5 fragments are poorly matched due to the relatively smaller *N*-substituents, which leads to the higher energies of the corresponding transition states.

To summarize, we have presented a mechanistic study on the Ni-catalyzed silylation and hydroarylation of arenes with vinylsilanes by means of DFT calculations. The selectivity is determined by the competition between C–Si and C–C reductive elimination, and NHC ligands play a critical role in differentiating the two pathways. The C–Si reductive elimination involves the four-coordinate intermediate, and the NHCs with less steric bulk favor the C–Si formation due to the small repulsions between the aryl and the ligand. Conversely, bulky NHCs in the T-shaped intermediate of the C–C reductive elimination exhibit better electrostatic matching with the substrate, thus promoting the C–C formation. The present results will provide important implications for future design of NHCs to control the selectivity.

This work was supported by National Natural Science Foundation of China (No. 21705075). The authors thank Dr. Jian-Biao Liu for helpful discussion.

View Article Online
DOI: 10.1039/C8CC04456B

Conflicts of interest

There are no conflicts to declare.

Notes and references

1 (a) Y. You, C. An, J. Kim and S. Y. Park, *J. Org. Chem.*, 2007, **72**, 6241–6246; (b) A. K. Franz and S. O. Wilson, *J. Med. Chem.*, 2013, **56**, 388–405; (c) E. Langkopf and D. Schinzer, *Chem. Rev.*, 1995, **95**, 1375–1408.

2 (a) P. D. Lickiss, *Adv. Inorg. Chem.,* 1995, **42**, 147–262; (b) S. E. Denmark and L. Neuville, *Org. Lett.*, 2000, **2**, 3221–3224.

3 M. Murata, M. Ishikura, M. Nagata, S. Watanabe, Y. Masuda, *Org. Lett.,* 2002, **4**, 1843–1845.

4 S. E. Denmark, R. C. Smith, W.-T. T. Chang, J. M. Muhuhi, *J. Am. Chem. Soc.,* 2009, **131**, 3104–3118.

5 (a) B. Marciniec, *Coord. Chem. Rev.*, 2005, **249**, 2374–2390; (b) H. F. Sore, W. R. J. D. Galloway and D. R. Spring, *Chem. Soc. Rev.*, 2012, **41**, 1845–1866; (c) C. Cheng and J. F. Hartwig, *Chem. Rev.*, 2015, **115**, 8946–8975.

6 (a) V. P. Ananikov, *ACS Catal.*, 2015, **5**, 1964–1971; (b) T. Sperger, I. A. Sanhueza, I. Kalvet and F. Schoenebeck, *Chem. Rev.*, 2015, **115**, 9532–9586; (c) C. Lin and P. P. Power, *Chem. Soc. Rev.*, 2017, **46**, 5347–5399; (d) G. Pototschnig, N. Maulide and M. Schnürch, *Chem. Eur. J.*, 2017, **23**, 9206–9232; (e) S. Z. Tasker, E. A. Standley and T. F. Jamison, *Nature*, 2014, **509**, 299–309; (f) X.-H. Cai and B. Xie, *ARKIVOC*, 2015, 184–211; (g) N. Chatani, *Top. Organomet. Chem.*, 2016, **56**, 19–46; (h) D. Janssen-Muller, C. Schlepphorst and F. Glorius, *Chem. Soc. Rev.*, 2017, **46**, 4845–4854; (i) *Catalytic Hydroarylation of Carbon-Carbon Multiple Bonds*; L. Ackermann, T. B. Gunnoe, L. G. Habgood, Eds.; Wiley-VCH Verlag GmbH & Co. KGaA: Weinheim, 2018; (j) S. A. Johnson, *Dalton Trans.*, 2015, **44**, 10905–10913; (k) V. Ritleng, M. Henrion and M. J. Chetcuti, *ACS Catal.*, 2016, **6**, 890–906.

7 For selected examples, see: (a) H. Wang, G. Lu, G. J. Sormunen, H. A. Malik, P. Liu and J. Montgomery, *J. Am. Chem. Soc.*, 2017, **139**, 9317–9324; (b) P. A. Donets and N. Cramer, *Angew. Chem., Int. Ed.*, 2014, **54**, 633–637; (c) S. Zhang, B. L. H. Taylor, C. Ji, Y. Gao, M. R. Harris, L. E. Hanna, E. R. Jarvo, K. N. Houk and X. Hong, *J. Am. Chem. Soc.*, 2017, **139**, 12994–13005; (d) C. Heinz, J. P. Lutz, E. M. Simmons, M. M. Miller, W. R. Ewing and A. G. Doyle, *J. Am. Chem. Soc.*, 2018, **140**, 2292–2300.

8 M. R. Elsby and S. A. Johnson, *J. Am. Chem. Soc.*, 2017, **139**, 9401–9407.

9 (a) J. Guihaumé, S. Halbert, O. Eisenstein and R. N. Perutz, *Organometallics*, 2012, **31**, 1300–1314; (b) S. Tang, O. Eisenstein, Y. Nakao and S. Sakaki, *Organometallics*, 2017, **36**, 2761–2771; (c) D. Balcells, E. Clot and O. Eisenstein, *Chem. Rev.*, 2010, **110**, 749–823.

10 S. R. Neufeldt, G. Jiménez-Osés, J. R. Huckins, O. R. Thiel and K. N. Houk, *J. Am. Chem. Soc.*, 2015, **137**, 9843–9854.

11 H. L. Schmider and A. D. Becke, *J. Mol. Struct. (THEOCHEM),* 2000, **527**, 51–61.

12 J. S. Bair, Y. Schramm, A. G. Sergeev, E. Clot, O. Eisenstein and J. F. Hartwig, *J. Am. Chem. Soc.*, 2014, **136**, 13098–13101.

13 M. N. Hopkinson, C. Richter, M. Schedler and F. Glorius, *Nature*, 2014, **510**, 485–496.

14 K. Tatsumi, R. Hoffmann, A. Yamamoto and J. K. Stille, *Bull. Chem. Soc. Jpn*, 1981, **54**, 1857–1867.

15 (a) V. P. Ananikov, D. G. Musaev and K. Morokuma, *Eur. J. Inorg. Chem.*, 2007, **2007**, 5390–5399; (b) P. Anstaett and F. Schoenebeck, *Chem. Eur. J.*, 2011, **17**, 12340–12346.

View Article Online
DOI: 10.1039/C8CC04456B

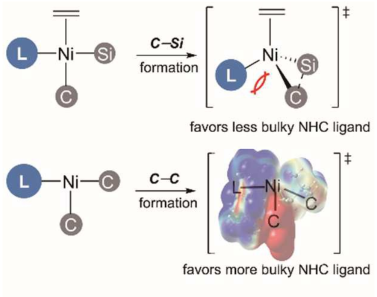

NHC controls the selectivity via different impacts on the C–Si/C–C reductive elimination of the square-planar/T-shaped intermediate.